

Analytical Model for GNSS Receiver Implementation Losses^{*}

Christopher J. Hegarty, *The MITRE Corporation*

BIOGRAPHY

Dr. Christopher J. Hegarty is a director with The MITRE Corporation, where he has worked mainly on aviation applications of GNSS since 1992. He is currently the Chair of the Program Management Committee of RTCA, Inc., and co-chairs RTCA Special Committee 159 (GNSS). He served as editor of *NAVIGATION: The Journal of the Institute of Navigation* from 1997 – 2006 and as president of the Institute of Navigation in 2008. He was a recipient of the ION Early Achievement Award in 1998, the U.S. Department of State Superior Honor Award in 2005, the ION Kepler Award in 2005, and the Worcester Polytechnic Institute Hobart Newell Award in 2006. He is a Fellow of the ION, and co-editor/co-author of the textbook *Understanding GPS: Principles and Applications*, 2nd Ed.

ABSTRACT

Global Navigation Satellite System (GNSS) receivers suffer signal-to-noise ratio (SNR) losses due to bandlimiting, quantization, and sampling. This paper presents an analytical model for GNSS receiver losses applicable to a wide variety of hardware configurations. The model addresses digitization of the received signal by a uniform quantizer with an arbitrary (even or odd) integer number of output levels. The model provides SNR loss values for GNSS signals in the presence of both additive white Gaussian noise and interference, provided that the interference can be accurately modeled as a non-white, Gaussian wide sense stationary process.

INTRODUCTION

Direct sequence spread spectrum (DSSS) receivers, including those used for the Global Navigation Satellite System (GNSS), suffer signal-to-noise ratio (SNR) losses due to bandlimiting, quantization, and sampling. Previous research into such losses has included: (1) low-fidelity analytical models that predict SNR loss values with many simplifying assumptions, (2) extensive simulation campaigns that provide useful loss values, but are time

intensive and do not provide much insight into the various loss mechanisms.

Earlier analytical studies of DSSS receiver SNR losses due to quantization include derivations in [1] for quantization losses of 1.96 dB and 0.55 dB, respectively, for 1- and 2-bit uniform quantizers. These derivations are simplified in that they assume that the received signal is sampled, but with independent noise upon each sample and ignoring bandlimiting effects on the desired signal component. A more thorough treatment of bandlimiting, sampling, and quantization effects in digital matched filters is provided in [2]. The results in [2] were later inferred to apply to GNSS receiver losses in [3, 4]. As detailed later in this paper, however, the results in [2] are truly not directly applicable to GNSS or other DSSS receivers because the losses derived therein presume coherent integration over only one symbol of the desired signal by the receiver, whereas DSSS receivers coherently integrate over many spreading symbols.

Monte Carlo simulation results for GNSS receiver SNR losses for a variety of modulation types, receiver configurations, and in the presence of both white noise and non-white interference are provided in [5] and [6]. These results, although useful, have several limitations. First, if loss results are required for a scenario not yet investigated, additional simulations must be run, and these can be extremely time intensive. A simulation tool developed by the second author of [5] and augmented in capability by others at MITRE takes over 6 hours on a desktop personal computer to yield results for a typical run. Second, simulations provide limited insights into the various mechanisms contributing towards implementation losses. Lastly, the loss results presented in [5, 6] are all for receivers using sampling rates that are commensurate with the desired GNSS signal symbol rates, i.e., with an integer number of samples per spreading symbol. As discussed within this paper, with commensurate sampling, receiver SNR losses are highly dependent on the phasing of the sampling epochs relative to the symbol transitions. Well-designed GNSS receivers avoid commensurate sampling rates, because of errors that can arise in pseudorange measurements when such rates are used [7, 8].

This paper presents an analytical model for GNSS receiver losses applicable to a wide variety of hardware configurations. The model addresses digitization of the received signal by a uniform quantizer with an arbitrary

^{*}The contents of this material reflect the views of the author. Neither the Federal Aviation Administration nor the Department of the Transportation makes any warranty or guarantee, or promise, expressed or implied, concerning the content or accuracy of the views expressed herein.

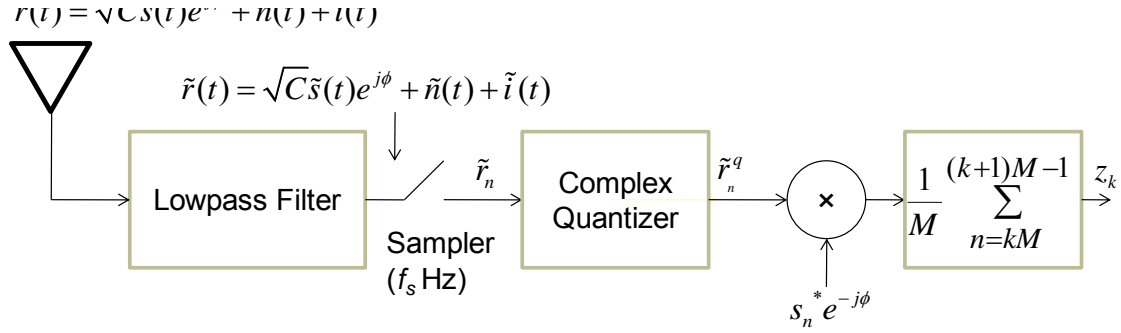


Figure 1. GNSS Receiver Signal Processing Model

(even or odd) integer number of output levels. The model includes the effects of sampling and bandlimiting, without limitations on the allowable sample rates or filter transfer functions. Both commensurate and non-commensurate sampling rates are considered, although as mentioned above the former are mostly of interest in comparing results with those reported previously in earlier studies.

As observed in the previous literature, losses are dependent on the desired signal modulation type. Furthermore, different losses are incurred for the three components of the received signal considered: (1) desired GNSS signal, (2) noise, and (3) Gaussian non-white interference (e.g., inter-/intra-system interference from a number of GNSS signals of the same or different modulation type). The analytical formulation provides insight into how implementation losses result from a combination of attenuation of the desired signal, and attenuation and/or enhancement of the noise/interference.

This paper is organized as follows. The analytical model is first derived and described in the following section, with certain cumbersome steps in the derivation relegated to appendices. The subsequent section provides implementation loss results from the analytical model and compares pertinent results against those found in the previous literature. The final section provides a short summary and conclusions.

ANALYTICAL MODEL

A simplified block diagram of signal processing within a GNSS receiver is shown in Figure 1. The received signal, $r(t)$, is modeled as the sum of a desired signal, noise $n(t)$, and interference $i(t)$. The baseband normalized (unity power) desired signal is denoted $s(t)$, with received phase ϕ (radians) and received power level of C watts. Note that Figure 1 is highly simplified and omits certain receiver processing functions that are considered lossless this analysis, e.g., down-conversion of the original L-band received signal to its in-phase (I) and quadra-phase (Q) components (treated here as a single complex signal).

The following subsections provide statistical models for the signal, noise, and interference, and then follow these received signal components through the processing shown in Figure 1. The final subsection derives expressions for

effective signal power and effective noise density at the output of the correlator, which when combined yield SNR losses.

Signal Model

The baseband normalized desired signal, $s(t)$, is modeled very generally as:

$$s(t) = \sqrt{\alpha} \sum_{l=-\infty}^{\infty} c_l p^{(l)}(t - lT_c) + j\sqrt{1-\alpha} \sum_{l=-\infty}^{\infty} d_l q^{(l)}(t - lT_c) \quad (1)$$

where α is the fraction of power in the signal's in-phase component, T_c is the symbol period, $\{c_l\}$ and $\{d_l\}$ are independent, white pseudorandom sequences from the binary alphabet $[-1, +1]$, and $p^{(l)}(t)$ and $q^{(l)}(t)$ are, respectively, the l -th spreading symbols used for the inphase and quadraphase components. The spreading symbols are real-valued and selected from finite sets,

$p^{(l)}(t) \in \{p_1(t), \dots, p_{N_p}(t)\}$, $q^{(l)}(t) \in \{q_1(t), \dots, q_{N_q}(t)\}$ with probabilities $P[p^{(l)}(t) = p_i(t)] \equiv P_{p_i}$ and

$P[q^{(l)}(t) = q_i(t)] \equiv P_{q_i}$. This definition is broad enough to apply to simple GNSS signals such as the GPS C/A code, for which there is only an in-phase component with all symbols taking on the same, rectangular shape, or to more complicated GNSS signals such as the GPS L1 civil signal (L1C) that include in- and quadra-phase components with a mixture of different symbols (the L1C pilot component uses two different symbol types that are time multiplexed).

The signal defined in equation (1) is cyclostationary, with a two-parameter autocorrelation function that is periodic with time, t , with period T_c :

$$\begin{aligned} R_s(t, \tau) &\equiv E[s(t+\tau)s^*(t)] \\ &= \alpha \sum_{n=1}^{N_p} P_{p_n} \sum_{l=-\infty}^{\infty} p_n(t - lT_c + \tau) p_n(t - lT_c) \\ &\quad + (1-\alpha) \sum_{n=1}^{N_q} P_{q_n} \sum_{l=-\infty}^{\infty} q_n(t - lT_c + \tau) q_n(t - lT_c) \end{aligned} \quad (2)$$

and its time-average may be defined as

$$R_s(\tau) \equiv \frac{1}{T_c} \int_0^{T_c} R_s(t, \tau) dt \quad (3)$$

$$= \alpha \sum_{n=1}^{N_p} P_{p_n} R_{p_n}(\tau) + (1-\alpha) \sum_{n=1}^{N_q} P_{q_n} R_{q_n}(\tau)$$

where

$$R_{p_n}(\tau) \equiv \frac{1}{T_c} \int_0^{T_c} p_n(t+\tau) p_n(t) dt \quad (4)$$

$$R_{q_n}(\tau) \equiv \frac{1}{T_c} \int_0^{T_c} q_n(t+\tau) q_n(t) dt$$

Noise and Interference Models

The noise, $n(t)$, and interference, $i(t)$, are assumed to be mutually independent, complex Gaussian wide sense stationary random processes. The noise is further assumed to be white with power spectral density of $S_n(f) = N_0$ watts/hertz (double-sided), whereas the interference has an arbitrary power spectral density $I \cdot S_i(f)$, where I is the received interference power level (watts), and $S_i(f)$ is the normalized (unity power) interference power spectrum.

Filtering

The low-pass filter in Figure 1 is specified by an arbitrary transfer function, $H(f)$. For some of the later results, an ideal low-pass filter with transfer function:

$$H(f) = \begin{cases} 1, & |f| < B/2 \\ 0, & \text{else} \end{cases} \quad (5)$$

is presumed, where B is the two-sided filter bandwidth. The filter outputs corresponding to each received signal component are denoted by tildes (e.g., $\tilde{s}(t), \tilde{n}(t), \tilde{i}(t)$).

For the transfer function specified in equation (5), after filtering the noise power spectral density is given by:

$$S_{\tilde{n}}(f) = \begin{cases} N_0, & |f| < B/2 \\ 0, & \text{else} \end{cases} \quad (6)$$

and its autocorrelation by:

$$R_{\tilde{n}}(\tau) \equiv E[\tilde{n}(t+\tau)\tilde{n}^*(t)] \quad (7)$$

$$= N_0 B \frac{\sin(\pi B\tau)}{(\pi B\tau)}$$

With ideal low-pass filtering as described by equation (5), the interference power spectral density is given by:

$$S_{\tilde{i}}(f) = \begin{cases} I \cdot S_i(f), & |f| < B/2 \\ 0, & \text{else} \end{cases} \quad (8)$$

For an arbitrary low-pass filter with transfer function $H(f)$, equations (6) and (8) may be replaced by the respective input noise and interference power spectral densities multiplied by $|H(f)|^2$.

It is assumed that within the receiver passband, the power of the desired signal is much lower than the combined power of the noise and interference, e.g., with ideal low-pass filtering,

$$C \int_{f=-B}^B S_s(f) df \ll N_0 B + I \int_{f=-B}^B S_i(f) df \quad (9)$$

where $S_s(f)$ is the Fourier transform of $R_s(\tau)$.

Sampling

The low-pass filtered received signal is uniformly sampled at rate f_s . After sampling, the received signal may be expressed as:

$$\tilde{r}_n \equiv \tilde{r}(t_n) \quad (10)$$

$$= \tilde{r}(nT_s + T_0)$$

where $T_s = 1/f_s$ is the sampling period, and T_0 is a constant timing offset.

The autocorrelation of the sampled received signal may be expressed as:

$$R_{\tilde{r}}[m] \equiv E[\tilde{r}(t_{n+m})\tilde{r}^*(t_n)] \quad (11)$$

$$= E[\tilde{r}_{n+m}\tilde{r}_n^*]$$

$$\approx R_{\tilde{n}}[m] + R_{\tilde{i}}[m]$$

where the last line follows from (9) and

$$R_{\tilde{i}}[m] \equiv R_{\tilde{i}}(mT_s) \quad (12)$$

$$= \int_{-\infty}^{\infty} S_{\tilde{i}}(f) e^{j2\pi fmT_s} df$$

The power spectral density of the sampled received signal is the discrete-time Fourier transform of (11), which can be expressed as a function of the continuous-time power spectral densities of the noise and interference components of the received signal, equations (6) and (8), respectively, as

$$S_{\tilde{r}}(e^{j\omega}) \equiv \sum_{m=-\infty}^{\infty} R_{\tilde{r}}[m] e^{-jm\omega} \quad (13)$$

$$\approx \frac{1}{T_s} \sum_{k=-\infty}^{\infty} \left[S_{\tilde{n}}\left(\frac{\omega f_s}{2\pi} - kf_s\right) + S_{\tilde{i}}\left(\frac{\omega f_s}{2\pi} - kf_s\right) \right]$$

where the approximation in the second line follows from the assumption stated in equation (9) that the noise and interference power are much larger than the desired signal power.

Quantizer

The complex quantizer in Figure 1 is modeled as shown in Figure 2, where $\text{Re}(\cdot)$ and $\text{Im}(\cdot)$ are the real and imaginary operators, respectively. \tilde{x}_n and \tilde{y}_n are introduced as the inphase and quadrature components of the received signal, respectively, and their quantized

versions are denoted by the same notation with a superscript , q '.

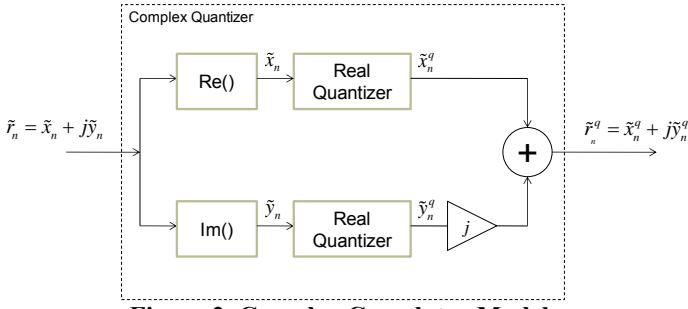


Figure 2. Complex Correlator Model

Each of the two real quantizers is modeled as an odd symmetric, memoryless nonlinearity whose output, $y(t)$, at arbitrary time, t , is only a function of the input voltage at that instant, $x(t)$, following the input-output characteristic [9]:

$$y(x) = K \cdot f(x) = K [f^+(x) - f^+(-x)] \quad (14)$$

$$f^+(x) = \sum_{p=1}^{\lfloor N/2 \rfloor} \delta_p u(x - a_p)$$

where N is the number of output levels, $u(x)$ is the unit step function, K is a gain constant and $\lfloor \cdot \rfloor$ is the floor operator whose output is the greatest integer less than or equal to its argument.

This paper focuses on quantizers with uniform step sizes. The input-output characteristic for a uniform quantizer is given by equation (14) with [9]

$$\begin{aligned} \delta_p &= Q/2 \cdot \varepsilon_{p-1} \\ a_p &= (p-1)Q \end{aligned} \quad (N \text{ even}) \quad (15)$$

or

$$\begin{aligned} \delta_p &= Q \\ a_p &= (p-1/2)Q \end{aligned} \quad (N \text{ odd}). \quad (16)$$

Examples for various values of N with $K = 1$ are shown in Figure 3.

For comparisons with previous studies, it is useful to note that the maximum input threshold, T , for an N level uniform quantizer is related to the parameter Q as:

$$T = \frac{(N-2)Q}{2} \quad (17)$$

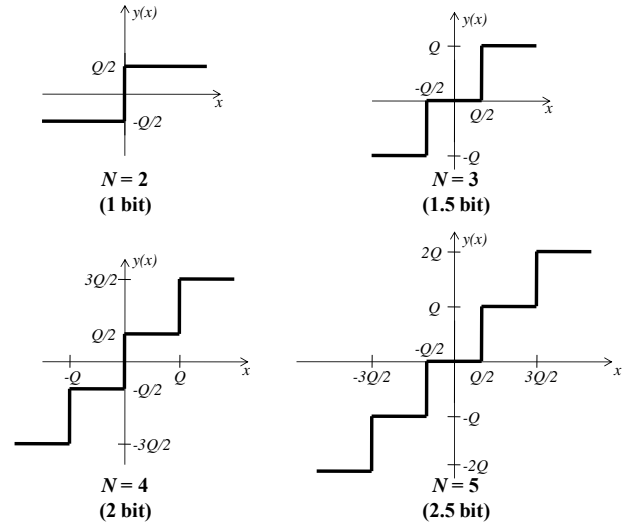


Figure 3. Examples of Uniform Quantizers

As derived in Appendix A, the autocorrelation of the output signal of the complex correlator may be related to the autocorrelation of the input signal utilizing results from [9, 10]. The result is:

$$R_{r^q}[m] = R_r[0] \sum_{k=1}^{\infty} \bar{b}_k \left[\left(\frac{\text{Re}[R_r[m]]}{R_r[0]} \right)^k + j \left(\frac{\text{Im}[R_r[m]]}{R_r[0]} \right)^k \right] \quad (18)$$

where

$$\bar{b}_k = \bar{K}^2 \cdot \bar{h}_{0k}^2 / k! \quad (19)$$

with the parameters \bar{h}_{0k} and \bar{K} defined as:

$$\bar{h}_{0k} = \begin{cases} 0, & k \text{ even} \\ \sqrt{2/\pi} \sum_{p=1}^{\lfloor N/2 \rfloor} \delta_p e^{-(a_p)^2/2} H_{k-1}(a_p), & k \text{ odd} \end{cases} \quad (20)$$

and

$$\bar{K} = \left(\sum_{k=1}^{\infty} \bar{h}_{0k}^2 / k! \right)^{-1/2} \quad (21)$$

In equation (20), $H_k(\cdot)$ is a k -th order Hermite polynomial. Efficient methods for numerically computing (20) and (21) are provided in Appendix A.

If the interference has a baseband power spectral density that is even symmetric, i.e., $S_i(f) = S_i(-f)$, then $R_r[m]$ will be entirely real for all m and thus:

$$R_{r^q}[m] = R_r[0] \sum_{k=1}^{\infty} \bar{b}_k \left(\frac{R_r[m]}{R_r[0]} \right)^k \quad (22)$$

The power spectral density of the complex quantizer output may be related to the power spectral density of its input by taking the discrete-time Fourier transform of equation (18):

$$S_{\tilde{r}^q}(e^{j\omega}) = R_{\tilde{r}}[0] \sum_{k=1}^{\infty} \bar{b}_k \left[\left(\frac{S_{\tilde{r}}(e^{j\omega}) + S_{\tilde{r}}(e^{-j\omega})}{2R_{\tilde{r}}[0]} \right)^{\otimes k} + j \left(\frac{S_{\tilde{r}}(e^{j\omega}) - S_{\tilde{r}}(e^{-j\omega})}{2jR_{\tilde{r}}[0]} \right)^{\otimes k} \right] \quad (23)$$

If the interference has a baseband power spectral density that is even symmetric, i.e., $S_I(f) = S_I(-f)$, such that $S_{\tilde{r}}(e^{j\omega}) = S_{\tilde{r}}(e^{-j\omega})$, then equation (23) reduces to:

$$S_{\tilde{r}^q}(e^{j\omega}) = R_{\tilde{r}}[0] \sum_{k=1}^{\infty} \bar{b}_k \left(\frac{S_{\tilde{r}}(e^{j\omega})}{R_{\tilde{r}}[0]} \right)^{\otimes k} \quad (24)$$

which may also be obtained by taking the discrete-time Fourier transform of equation (22).

Phase Rotation and Correlation

As shown in Figure 1, the received signal after filtering, sampling and quantization, \tilde{r}_n^q , is phase rotated by an estimate of the incoming signal phase (assumed here to be perfect) and then correlated against the complex conjugate of the discrete-time replica of the desired signal, s_n^* , resulting in the complex correlation sum:

$$z_k = \frac{1}{M} \sum_{n=kM}^{(k+1)M-1} \tilde{r}_n^q s_n^* e^{-j\phi} \quad (25)$$

where M is the number of samples per coherent correlation interval, $T_I = MT_s$.

As derived in Appendix B, the mean value of the k -th complex correlation sum is:

$$E[z_k] = \bar{K} \cdot \bar{h}_{01} \cdot \sqrt{C} \cdot \bar{R}_{ss}(0) \quad (26)$$

where

$$\bar{R}_{ss}(\tau) \equiv \frac{1}{M} \sum_{n=kM}^{(k+1)M-1} R_{ss}(t_n; \tau) \quad (27)$$

is the time-average (over sample epochs across the coherent correlation interval) of the two-parameter cross-correlation function between the filtered and unfiltered desired signal, i.e.,

$$\begin{aligned} R_{ss}(t; \tau) &\equiv E[\tilde{s}(t+\tau)s^*(t)] \\ &= \alpha \sum_{n=1}^{N_p} P_{p_n} \sum_{l=-\infty}^{\infty} \tilde{p}_n(t+\tau)p_n(t) \\ &\quad + (1-\alpha) \sum_{n=1}^{N_q} P_{q_n} \sum_{l=-\infty}^{\infty} \tilde{q}_n(t+\tau)p_n(t) \end{aligned} \quad (28)$$

with

$$\begin{aligned} \tilde{p}_n(t) &= h(t) \otimes p_n(t) \\ \tilde{q}_n(t) &= h(t) \otimes q_n(t) \\ h(t) &= \mathfrak{F}^{-1}\{H(f)\} \end{aligned} \quad (29)$$

where $h(t)$ is the impulse response of the low-pass filter in Figure 1, equal to the inverse Fourier transform of its transfer function, $H(f)$. For the transfer function provided in equation (5),

$$h(t) = 2B \frac{\sin(2\pi Bt)}{2\pi Bt} \quad (30)$$

As mentioned in the introduction, well-designed receivers use sample rates that are incommensurate with the spreading symbol rate [7, 8]. With incommensurate sample rates, equation (27) is well-approximated by:

$$\begin{aligned} \bar{R}_{ss}(\tau) &= \frac{1}{T_c} \int_0^{T_c} R_{ss}(t; \tau) dt \\ &= R_s(\tau) \otimes h(\tau) \end{aligned} \quad (31)$$

since over the coherent correlation interval, the sampling epochs t_n are uniformly distributed across the spreading symbols. It follows then, that for incommensurate sampling rates:

$$\bar{R}_{ss}(0) = \int_{f=-\infty}^{\infty} H(f)S_s(f)df \quad (32)$$

in general, and

$$\bar{R}_{ss}(0) = \int_{f=-B/2}^{B/2} S_s(f)df \quad (33)$$

for the ideal filter with transfer function provided in equation (5).

Another case worthy of special note is when the sample rate is exactly commensurate with the spreading symbol rate:

$$f_s = \frac{N_s}{T_c} \quad (34)$$

where N_s is a positive integer representing the number of samples per spreading symbol. Although commensurate sampling is rarely found in GNSS receivers, it has been assumed in previous studies [2, 5, 6] and its treatment in this paper has been included to facilitate a comparison of results.

Commensurate sampling is illustrated in Figure 5. At the top of the figure is the desired signal component of the baseband received signal with rectangular symbols after filtering. The bottom of the figure indicates the sampling epochs. Note that there are exactly two samples per symbol. The phasing of the sample epochs with respect to the symbol transitions is captured by the time offset parameter, T_0 , introduced in equation (10). In Figure 5, $T_0 = 0$, i.e., the first of every two samples coincides with the leading edge of a symbol.

With commensurate sampling,

$$\bar{R}_{ss}(\tau) = \frac{1}{N_s} \sum_{n=0}^{N_s-1} R_{ss}(nT_s + T_0; \tau) \quad (35)$$

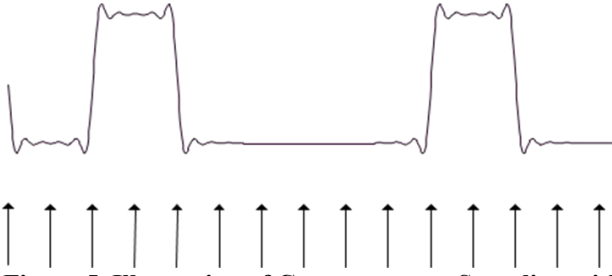


Figure 5. Illustration of Commensurate Sampling with Two Samples per Spreading Symbol

The variance of the k -th complex correlation sum, as derived in Appendix B, may be accurately approximated for $MT_s \gg T_c$ as:

$$\begin{aligned} \text{var}[z_k] &\approx \frac{1}{M} \sum_{n=-(M-1)}^{M-1} R_{\tilde{r}^q}[n]R_s[n] \\ &= \frac{1}{M} \frac{1}{2\pi} \int_{-\pi}^{\pi} S_{\tilde{r}^q}(e^{j\omega})S_s(e^{j\omega})d\omega \end{aligned} \quad (36)$$

Signal-to-noise Loss

Using equation (26), the effective signal power at the output of the correlator may be found as:

$$\begin{aligned} (C)_{\text{eff}} &= |E[z_k]|^2 = (\bar{K} \cdot \bar{h}_{01})^2 \bar{R}_{ss}^2(0) \cdot C \\ &= C / L_c \end{aligned} \quad (37)$$

where

$$L_c = \frac{1}{[\bar{K} \cdot \bar{h}_{01} \cdot \bar{R}_{ss}(0)]^2} \quad (38)$$

represents the loss in signal power due to bandlimiting, sampling, and quantization as can be observed by noting that $(C)_{\text{eff}} = C$ in the limit as the filter bandwidth $B \rightarrow \infty$, the sample rate $f_s \rightarrow \infty$, and the quantizer levels $N \rightarrow \infty$ such that in Figure 1, $\tilde{r}_n^q \approx \sqrt{C} s_n e^{j\phi} + n_n + i_n$.

Signal losses for a variety of quantizer levels, N , and as a function of maximum input threshold level, T , are shown in Figure 4 and minimum signal loss values and associated quantizer thresholds are summarized in Table 1. In both Figure 3 and Table 1, the results presume that the receiver bandwidth is sufficiently wide and the sampling frequency is sufficiently high so that the desired signal component of the received signal is negligibly attenuated, i.e., $\bar{R}_{ss}(0) \approx 1$. If this condition does not hold, an additional loss due to bandlimiting must be applied, utilizing equation (32) for incommensurate sampling or equation (35) for commensurate sampling.

The effective noise plus interference power density is given by:

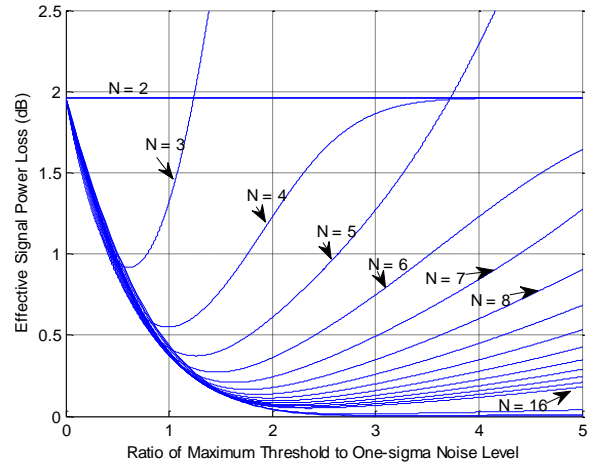


Figure 4. Signal Losses for Quantizers with N Levels vs. Maximum Input Threshold

Table 1. Minimum Signal Loss Values and Quantizer Threshold Settings

Number of Quantizer Levels, N	Minimum Signal Loss (dB)	Optimum Threshold Parameter, Q	Optimum Maximum Input Threshold Level, T
2	1.961	N/A	N/A
3	0.916	1.224	0.612
4	0.549	0.996	0.996
5	0.372	0.843	1.265
6	0.272	0.733	1.466
7	0.208	0.651	1.628
8	0.166	0.586	1.758
16	0.050	0.335	2.345
32	0.015	0.188	2.820
64	0.005	0.104	3.224
128	0.001	0.057	3.591

$$(N_0)_{\text{eff}} = \frac{T_s}{2\pi} \int_{-\pi}^{\pi} S_{\tilde{r}^q}(e^{j\omega})S_s(e^{j\omega})d\omega \quad (39)$$

since in the presence of desired signal plus noise only, as is well-known, the correlation sum variance must equal N_0 / T_s and thus (36) must equal $N_0 / T_s = N_0 / (MT_s)$ in the limiting conditions ($B \rightarrow \infty, f_s \rightarrow \infty, N \rightarrow \infty$).

RESULTS AND VALIDATION

Rectangular Symbols, Ideal Filtering, Nyquist Sample Rate, Noise-only

Some simplifications to the analytical model are possible when the sampling rate is equal to the two-sided receiver

bandwidth, $f_s = B$, only noise is considered, and ideal filtering as described by equation (5) is employed. In these conditions, the noise component of the sampled received signal is white, i.e., $R_{\tilde{r}_i}[m] = N_0 B \delta_m$. From equation (22), the output of the complex quantizer for any number of levels has the same autocorrelation function, $R_{\tilde{r}_q}[m] = N_0 B \delta_m$. It follows then that $S_{\tilde{r}_q}(e^{j\omega}) = N_0 f_s$ and substitution of this result into equation (17) yields $(N_0)_{eff} = N_0$. The SNR loss, thus, under these conditions is entirely attributable to the effective signal loss provided by equation (18).

Figures 6 and 7 present SNR loss results from the analytical model for a desired signal using rectangular symbols, ideal filtering as described in equation (5), Nyquist rate sampling, and thermal noise only. Figure 6 shows losses when the two-sided receiver bandwidth is equal to twice the chipping rate, $B = 2/T_c$. This case is applicable, e.g., to a C/A-code receiver with a 2.046 MHz two-sided bandwidth or a L5 receiver with a 20.46 MHz two-sided bandwidth. In this case, there are exactly two samples per spreading symbol in the desired signal. The sampling time offset, T_0 , in equation (8) was selected to be $T_c/4$, so that the two samples per symbol were centered with respect to the symbol minimizing signal loss.

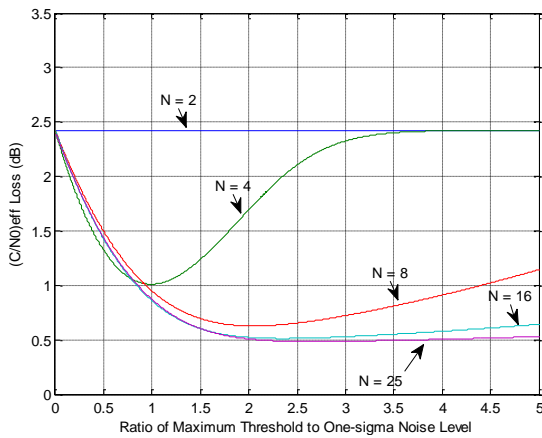


Figure 6. SNR Losses – Rectangular Symbols, Noise Only, Two-sided Receiver Bandwidth Equal to Twice the Chipping Rate, Nyquist Sample Rate

Figure 7 plots losses when the two-sided bandwidth is ten times the chipping rate, $B = 10/T_c$, e.g., a C/A-code receiver with a 10.23 MHz two-sided bandwidth. Nyquist sampling was used resulting in ten samples per spreading symbol with $T_0 = T_c/20$, so that the ten samples in each symbol are centered with respect to the start and end of the symbol.

The results in Figures 6 and 7 were originally of concern, since they are significantly different than the results for the same scenario as reported in two prominent texts [3] and [4], which both provide SNR loss values that originate from [2]. As an example of the differences, [2] indicates a 3.47 dB SNR loss with a 1-bit quantizer for the

conditions used to produce Figure 5, whereas the analytical model indicates an SNR loss of 2.42 dB.

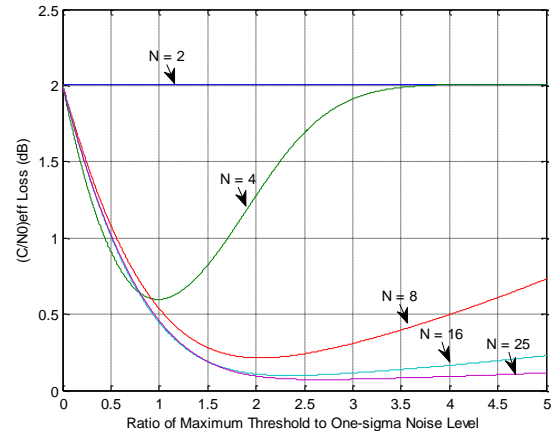


Figure 7. SNR Losses – Rectangular Symbols, Noise Only, Two-sided Receiver Bandwidth Equal to Ten Times the Chipping Rate, Nyquist Sample Rate

Upon further study, it is clear that the SNR loss results in [2], without extension, are not truly applicable to GNSS receivers. The reason for this is that the results in [2] are focused on a communications receiver that only coherently integrates over one symbol. GNSS receivers typically coherently integrate over many spreading symbols. For example, a C/A-code receiver typically integrates over at least 1023 spreading symbols (chips) for all modes of operation.

The method used in [2] to compute SNR losses is to first determine the probability mass function for each quantized sample of the received signal. With Nyquist sampling, as explained at the beginning of this section, noise samples are independent of each other. Thus, with an integer number of samples per symbol in a digital matched filter, it is possible to determine the probability mass function of the sum of quantized samples as integrated over each symbol by convolving the per-sample probability mass functions. The method in [2] can be extended for a receiver that coherently integrates over many symbols simply by further convolving the probability mass function obtained for one symbol over as many symbols as are included within the coherent integration period.

Figure 8 shows SNR losses as a function of the number of symbols within the coherent integration period for the conditions used to produce Figure 6. Figure 8 was produced using the extension of the method in [2] outlined above and with the quantizer thresholds shown in Table 1. As the number of symbols in the coherent integration period is increased, the SNR loss results asymptote to the values predicted by the analytical model (which presumes a coherent integration period that is much longer than the spreading symbol period). Tables 2 and 3 summarize a comparison of SNR loss results from this extension of the method from [2] vs. results from the analytical model described in this paper. Note the

excellent agreement, with all results between the two vastly different methods equal to within 0.01 dB.

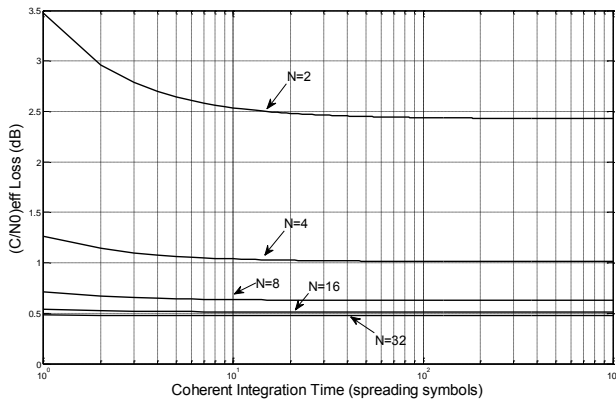


Figure 8. SNR Loss Results Using Extension of Method in [2]; Rectangular Symbols, Noise Only, Two-sided Receiver Bandwidth Equal to Twice the Chipping Rate, Nyquist Sample Rate

Table 2. Comparison of SNR Loss Results from Extension of Method in [2] vs. Analytical Model; Rectangular Symbols, Noise Only, Two-sided Receiver Bandwidth Equal to Twice the Chipping Rate, Nyquist Sample Rate

Number of Quantizer Levels, N	Minimum Loss per Extension of Method in [2] (dB)*	Minimum Loss per Analytical Model (dB)
2	2.43	2.42
4	1.01	1.01
8	0.63	0.63
16	0.51	0.51
25	0.48	0.48

*With coherent integration period = 1000 symbols.

Table 3. Comparison of SNR Loss Results from Extension of Method in [2] vs. Analytical Model; Rectangular Symbols, Noise Only, Two-sided Receiver Bandwidth Equal to Ten Times the Chipping Rate, Nyquist Sample Rate

Number of Quantizer Levels, N	Minimum Loss per Extension of Method in [Chang] (dB)*	Minimum Loss per Analytical Model (dB)
2	2.01	2.01
4	0.60	0.60
8	0.21	0.21
16	0.10	0.10
25	0.07	0.07

*With coherent integration period = 1000 symbols.

It should be noted that when commensurate sampling is used with a small number of samples per spreading symbol, SNR losses are highly dependent upon the relative phasing between the sample epochs and desired signal symbol edges. Figure 9 illustrates the sensitivity by plotting loss results vs. the timing offset T_0 for a one-bit ($N = 2$) quantizer, Nyquist sample rate, rectangular symbols, and ideal filtering with two sided bandwidth of twice the chip rate. These results can best be understood by viewing Figure 5. With two samples per spreading symbol, minimum signal power losses occur when the two samples are centered with respect to each symbol. If T_0 is zero, the first of the two samples is aligned with the symbol leading edge, which is zero half the time (every time the preceding symbol has the opposite polarity). The net result is that on average 1 of 4 samples is devoid of energy from the desired signal component and the receiver suffers an approximate 1.3 dB additional loss for $T_0 = 0$ vs $T_0 = T_s/2$. Optimum sample phasing was explicitly utilized in [2] and in the results presented in Tables 2 and 3, whereas worst-case phasing is apparent from the loss results presented in [5,6].

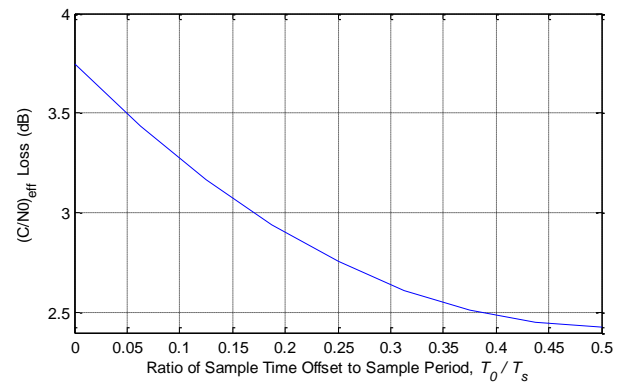


Figure 9. SNR Loss Sensitivity to Sampling Epoch Phasing with Commensurate Sampling

Validation

To validate the analytical model, SNR loss results were computed for 17 scenarios and compared with Monte Carlo simulations using a tool developed originally by the second author of [3] and significantly further developed by Dr. Alex Cerruti of MITRE. The scenarios included a wide variety of desired binary phase shift keyed (BPSK) and binary offset carrier (BOC) signal modulation types, quantizer levels, receiver bandwidths, and sample rates. In the description to follow the notation BPSK-R(n) is used for a BPSK signal with an $n \times 1.023$ MHz symbol (chipping) rate and rectangular symbols. BOC(m,n) denotes a BOC modulation with a $m \times 1.023$ MHz square wave subcarrier and a $n \times 1.023$ MHz symbol rate. TMBOC denotes the time multiplexed BOC modulation that will be used for the pilot component of the GPS L1 Civil (L1C) signal that time multiplexes 29 BOC(1,1) symbols and 4 BOC(6,1) symbols out of every 33 total symbols.

Figure 8 plots the results of the first scenario, which represents aggregate BOC(10,5) interference to a victim BPSK-R(1) receiver. White thermal noise was also present. The interference-to-noise density was varied over 20 values from $-\infty$ to 108 dB. The receiver had a -6 dB two-sided bandwidth of 2.0 MHz with attenuation provided by a 12-th order Butterworth filter (the cascade of two 6-th order filters with -3 dB bandwidths of 2.0 MHz), and digitized the received signal, noise, and interference with a 2.0 MHz sample rate and with one-bit quantization. Each simulation result point in Figure 8 is based upon Monte Carlo simulation of 100,000 complex correlation sums with a 1-ms coherent integration time. The analytical model was carefully tuned to the scenario, using the transfer function of the true digital filter that was used in the simulations. The analytical model also used an aliased power spectrum for the input desired signal and aggregate interference since the simulations created these digitally with an original sampling rate of 163.68 MHz. Nearest-neighbor resampling was used in the simulations to decimate from the original high sampling rate to the final receiver sample rate, and this was accounted for in the analytical model utilizing an equivalent signal processing model where the high rate sampled signal is converted to analog using a sample-and-hold, with its well known distortion to the signal spectrum, and then resampled. Three desired signal powers were evaluated. The analytical results very closely matched the simulation results with an average error below 0.01 dB, and a peak error of 0.12 dB.

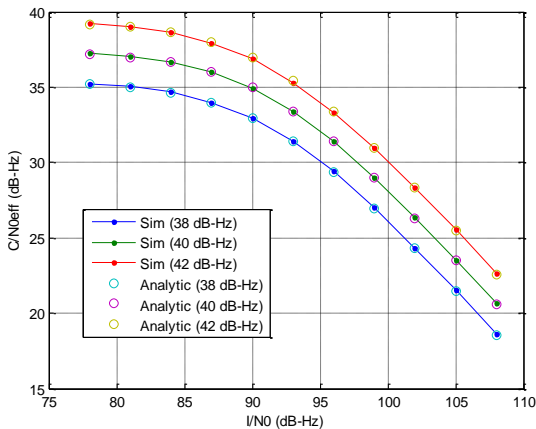


Figure 8. BOC(10,5) on BPSK-R(1) Scenario Results

The remaining 16 scenarios were run with only 10,000 1-ms coherent correlation sums per simulation data point due to time considerations. The results for a few of the scenarios are shown in Figures 9 – 11. Overall, the simulation and analytical model results were in excellent agreement, with typical differences less than a few tenths of a dB for effective C/N_0 's down to around 20 dB-Hz. This level of error is attributable to the natural variation of the Monte Carlo simulations with 10,000 correlation sums per data point. At lower effective C/N_0 's, larger differences were observed but deduced to be due to the increased variance of the simulation loss estimates with

decreased SNR, as demonstrated through additional simulation runs for a select number of points.

One scenario involving aggregate cosine-phased BOC(15,2.5) interference to a narrow-band BPSK-R(1) receiver resulted in abnormally large differences between the simulation results and the analytical results. Debugging of the scenario revealed that the filter transfer function that was applied in the analytical model did not truly match the attenuation that occurred within the simulation tool. MATLAB was used for the simulations, and the MATLAB `filtfilt.m` function was found to have significant dynamic range problems, resulting in the filtered received signal power spectral density being much higher than would be predicted using the filter transfer function provided by another MATLAB function, `freqz.m`. This problem only manifested itself in one of the sixteen scenarios, because this particular scenario had an extremely low degree of overlap between the interference and the desired signal power spectra. Since the objective of the comparison exercise was to validate the analytical model, and the discrepancy in results was found to be due to problems with the simulation tool, this particular scenario was dropped from further analysis.

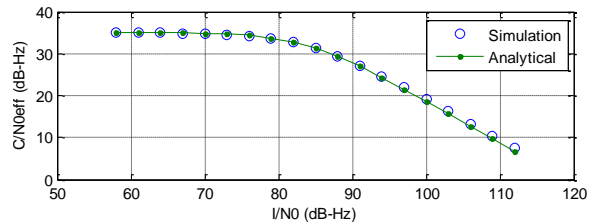


Figure 9. BOC(14,2) on BOC(10,5) Scenario Results; 2-bit Quantization, 24.0 MHz Two-sided Receiver Bandwidth, 24.0 MHz Sample Rate

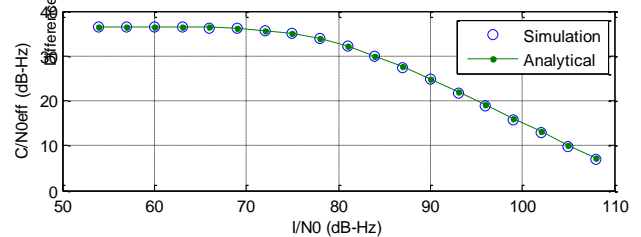


Figure 10. BOC(10,5) on BPSK-R(10) Scenario Results; 2-bit Quantization, 24.0 MHz Two-sided Receiver Bandwidth, 24.0 MHz Sample Rate

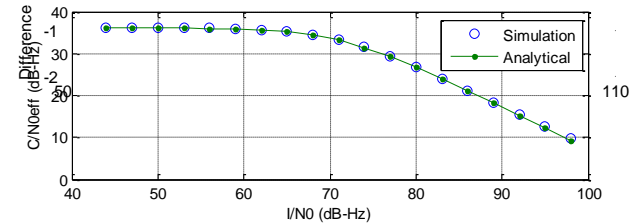


Figure 11. TMBOC on BPSK-R(10) Scenario Results; 1.5-bit (3-level) Quantization, 20.0 MHz Two-sided Receiver Bandwidth, 20.0 MHz Sample Rate

SUMMARY AND CONCLUSIONS

This paper has presented an analytical model for the computation of implementation losses suffered by GNSS receivers due to bandlimiting, sampling, and quantization. The model has been shown to accurately predict SNR losses due to bandlimiting, sampling, and quantization. It has the distinct advantage over Monte Carlo simulations in that it allows rapid determination of losses for scenarios not yet considered.

APPENDIX A: OUTPUT AUTOCORRELATION AND POWER SPECTRAL DENSITY OF A COMPLEX QUANTIZER WITH WIDE-SENSE-STATIONARY GAUSSIAN INPUT

The autocorrelation $R_y(\tau)$ of the output signal $y(t)$ of a memoryless nonlinearity driven by a zero-mean, Gaussian, wide-sense stationary random process $x(t)$ with autocorrelation function $R_x(\tau)$ may be generally expressed as [10]:

$$R_y(\tau) = \sum_{k=1}^{\infty} b_k R_x^k(\tau) \quad (\text{A-1})$$

where the coefficients $\{b_k\}$ are a function of the specific nonlinearity. A variety of methods for determining the coefficients are provided in [10]. The coefficients for a uniform quantizer with input-output characteristics as described in equation (2-14) may be expressed as:

$$b_k = K^2 \cdot h_{0k}^2 / k! \quad k \text{ even}$$

$$h_{0k} = \begin{cases} 0, & k \text{ even} \\ \sqrt{2/\pi} \frac{1}{\sigma_x^k} \sum_{p=1}^{\lfloor N/2 \rfloor} \delta_p e^{-(a_p/\sigma_x)^2/2} H_{k-1}(a_p/\sigma_x), & k \text{ odd} \end{cases} \quad (\text{A-2})$$

where $\sigma_x^2 \equiv R_x(0)$ is the power of the input process and $H_k(x)$ is a k -th order Hermite polynomial defined as:

$$H_k(x) \equiv (-1)^k \exp(x^2/2) \frac{d^k}{dx^k} \exp(-x^2/2). \quad (\text{A-3})$$

Equation (A-2) is easily derived from a more general result for the output autocorrelation of a uniform quantizer driven by the sum of Gaussian noise and an unmodulated carrier from [9]. It is noted in [9] that the output autocorrelation function of a uniform quantizer driven only by additive Gaussian noise (as used in this report) was derived earlier by Velichkin, but the reference cited in [9] for this prior work could not be located for use herein. For $N = 2$, the coefficients in (A-2) are a series expansion of the arctangent function [11].

The gain constant K is selected to achieve unity power gain for the quantizer, i.e., such that:

$$\sigma_y^2 \equiv R_y(0) = \sigma_x^2 \quad (\text{A-4})$$

Using equations (A-1) and (A-2), the condition stated in (A-4) requires that:

$$K = \left(\sum_{k=1}^{\infty} h_{0k}^2 \sigma_x^{2k-2} / k! \right)^{-1/2} \quad (\text{A-5})$$

The power spectrum of the quantizer output signal may be related to the power spectrum of the input signal by taking the Fourier transform of both sides of equation (A-1) yielding:

$$S_y(f) = \sum_{k=1}^{\infty} b_k [S_x(f)]^{\otimes k} \quad (\text{A-6})$$

where the notation $[S_x(f)]^{\otimes k}$ denotes the convolution of the input power spectrum $S_x(f)$ by itself k times.

The results of equation (A-1) and (A-6) are readily adapted to discrete-time signals. For instance, as applied to the in-phase discrete-time signal, \tilde{x}_n , from Figure 2:

$$R_{\tilde{x}^q}[m] = \sum_{k=1}^{\infty} b_k R_{\tilde{x}}^k[m] \quad (\text{A-7})$$

and

$$S_{\tilde{x}^q}(e^{j\omega}) = \sum_{k=1}^{\infty} b_k [S_{\tilde{x}}(e^{j\omega})]^{\otimes k} \quad (\text{A-8})$$

where it is understood in equation (A-8) that the convolution is now circular as appropriate for discrete-time signals, e.g.,

$$[S_{\tilde{x}}(e^{j\omega})]^{\otimes 2} = S_{\tilde{x}}(e^{j\omega}) \otimes S_{\tilde{x}}(e^{j\omega})$$

$$= \frac{1}{2\pi} \int_{-\pi}^{\pi} S_{\tilde{x}}(e^{j\theta}) S_{\tilde{x}}(e^{j(\omega-\theta)}) d\theta. \quad (\text{A-9})$$

It is useful numerically to replace the model for each real quantizer with an equivalent model shown in Figure A-1. In this figure, (a) and (b) are equivalent provided that the quantizer input/output levels are adjusted to maintain constant ratios with respect to the input signal standard deviations, i.e., if a quantizer parameter Q is used in (a), (b) must use the quantizer parameter $Q/\sigma_{\tilde{x}}$.

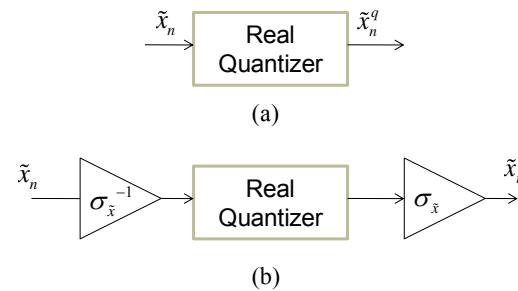


Figure A-1. Equivalent Models for a Real Quantizer

The equivalence of (a) and (b) in Figure A-1 may be demonstrated by rewriting equation (A-7) as:

$$R_{\tilde{x}^q}[m] = \sum_{k=1}^{\infty} b_k \sigma_{\tilde{x}}^{2k} \left(\frac{R_{\tilde{x}}[m]}{\sigma_{\tilde{x}}^2} \right)^k \quad (\text{A-10})$$

$$= \sigma_{\tilde{x}}^2 \sum_{k=1}^{\infty} \bar{b}_k \left(\frac{R_{\tilde{x}}[m]}{\sigma_{\tilde{x}}^2} \right)^k$$

where

$$\bar{b}_k = b_k \sigma_{\tilde{x}}^{2k-2} \quad (\text{A-11})$$

$$= \bar{K}^2 \cdot \bar{h}_{0k}^2 / k!$$

with the parameters \bar{h}_{0k} and \bar{K} defined as:

$$\bar{h}_{0k} = h_{0k} \sigma_{\tilde{x}}^k$$

$$= \begin{cases} 0, & k \text{ even} \\ \sqrt{2/\pi} \sum_{p=1}^{\lfloor N/2 \rfloor} \delta_p e^{-(a_p)^2/2} H_{k-1}(a_p), & k \text{ odd} \end{cases} \quad (\text{A-12})$$

and

$$\bar{K} = K / \sigma_{\tilde{x}}$$

$$= \left(\sum_{k=1}^{\infty} h_{0k}^2 \sigma_{\tilde{x}}^{2k} / k! \right)^{-1/2} \quad (\text{A-13})$$

$$= \left(\sum_{k=1}^{\infty} \bar{h}_{0k}^2 / k! \right)^{-1/2}$$

The second line of equation (A-10) validates the equivalence of Figure A-1 (a) and (b) since the summation in this line is seen to be the autocorrelation of the output of a real quantizer (see equation A-7) with the input signal $\tilde{x}_n / \sigma_{\tilde{x}}$. The autocorrelation is increased by $\sigma_{\tilde{x}}^2$ after the gain factor of $\sigma_{\tilde{x}}$ following the real quantizer in Figure A-1 (b).

Using this equivalent model, the power spectral density in (A-8) may be rewritten as:

$$S_{\tilde{x}^q}(e^{j\omega}) = \sigma_{\tilde{x}}^2 \sum_{k=1}^{\infty} \bar{b}_k \left[\frac{S_{\tilde{x}}(e^{j\omega})}{\sigma_{\tilde{x}}^2} \right]^{\otimes k} \quad (\text{A-14})$$

The output autocorrelation function for the complex quantizer in Figure 2 may be found as:

$$R_{\tilde{r}^q}[m] \equiv E \left[\tilde{r}_{m+n}^q (\tilde{r}_n^q)^* \right]$$

$$= E \left[(\tilde{x}_{m+n}^q + j\tilde{y}_{m+n}^q) (\tilde{x}_n^q - j\tilde{y}_n^q) \right] \quad (\text{A-15})$$

$$= R_{\tilde{x}^q}[m] - jR_{\tilde{x}^q\tilde{y}^q}[m] + jR_{\tilde{y}^q\tilde{x}^q}[m] + R_{\tilde{y}^q}[m]$$

The first and last terms of the last line of (A-15) are provided by equation (A-7).

The two middle terms of (A-15) can be determined by observing that the derivation of (A-1) from [10] applies to the cross-correlation between any pair of random variables before and after the same memoryless nonlinearity, $Kf(x)$, is applied to each of the two variables. Let X_1 and X_2 be a pair of random variables and let $Y_1 = Kf(X_1)$ and $Y_2 = Kf(X_2)$. Equation (A-1) results from selecting:

$$X_1 = x(t + \tau) \quad (\text{A-16})$$

$$X_2 = x(t)$$

It follows then, that by selecting:

$$X_1 = \tilde{x}_{n+m} \quad (\text{A-17})$$

$$X_2 = \tilde{y}_m$$

Then,

$$R_{\tilde{x}^q\tilde{y}^q}[m] = \sum_{k=1}^{\infty} b_k \left(R_{\tilde{y}\tilde{x}}[m] \right)^k \quad (\text{A-18})$$

Substituting (A-7) and (A-18) into (A-15) yields:

$$R_{\tilde{r}^q}[m] = R_{\tilde{x}^q}[m] - jR_{\tilde{x}^q\tilde{y}^q}[m] + jR_{\tilde{y}^q\tilde{x}^q}[m] + R_{\tilde{y}^q}[m]$$

$$= \sum_{k=1}^{\infty} b_k \left(R_{\tilde{x}}^k[m] - jR_{\tilde{y}\tilde{x}}^k[m] + jR_{\tilde{x}\tilde{y}}^k[m] + R_{\tilde{y}}^k[m] \right) \quad (\text{A-19})$$

Based upon earlier assumptions that the noise and interference are zero-mean and wide sense stationary, and further that these received signal components dominate the desired signal, the cross-correlation of the received signal in-phase and quadrature components must satisfy certain constraints [12]:

$$R_{\tilde{y}\tilde{x}}[m] = -R_{\tilde{x}\tilde{y}}[m] = R_{\tilde{y}\tilde{x}}[-m] \quad (\text{A-20})$$

$$R_{\tilde{x}}[m] = R_{\tilde{y}}[m]$$

Using these relationships, (A-19) may be simplified as:

$$R_{\tilde{r}^q}[m] = \sum_{k=1}^{\infty} b_k \left(R_{\tilde{x}}^k[m] - jR_{\tilde{y}\tilde{x}}^k[m] + jR_{\tilde{x}\tilde{y}}^k[m] + R_{\tilde{y}}^k[m] \right)$$

$$= \sum_{k=1}^{\infty} b_k \left(2R_{\tilde{x}}^k[m] + j \left[1 - (-1)^k \right] R_{\tilde{x}\tilde{y}}^k[m] \right) \quad (\text{A-21})$$

$$= 2 \sum_{k=1}^{\infty} b_k \left(R_{\tilde{x}}^k[m] + jR_{\tilde{x}\tilde{y}}^k[m] \right)$$

where (A-2) was used (specifically, the fact that for a uniform quantizer $b_k = 0$ for k even) going from the second to the last line of (A-21).

Equation (A-21) may be simplified further by noting that the autocorrelation of the input to the complex quantizer, $R_{\tilde{r}}[m]$, may be expanded as:

$$R_{\tilde{r}}[m] \equiv E \left[\tilde{r}_{m+n} (\tilde{r}_n)^* \right]$$

$$= E \left[(\tilde{x}_{m+n} + j\tilde{y}_{m+n}) (\tilde{x}_n - j\tilde{y}_n) \right] \quad (\text{A-22})$$

$$= R_{\tilde{x}}[m] - jR_{\tilde{y}\tilde{x}}[m] + jR_{\tilde{x}\tilde{y}}[m] + R_{\tilde{y}}[m]$$

$$= 2R_{\tilde{x}}[m] + 2jR_{\tilde{x}\tilde{y}}[m]$$

The final result, relating the autocorrelation of the output of the complex quantizer to the autocorrelation of its input is presented in the main body of this paper as equation (18) and the input-output relationships for power spectral densities is presented in the main body as equation (23).

Numerical Considerations

Determining the $\{b_k\}$ coefficients in (A-2) requires numerical computation of Hermite polynomials and $k!$, both of which can lead to overflow problems for large k . These may be avoided by noting that although the

numerator and denominator of b_k grow exceedingly large with k , the ratio does not.

The k -th order Hermite polynomial, $H_k(x)$, is defined in (A-3). The polynomials for $k = 0$ and $k = 1$ may be readily found as:

$$\begin{aligned} H_0(x) &= 1 \\ H_1(x) &= x \end{aligned} \quad (\text{A-23})$$

Higher order Hermite polynomials may be efficiently computed using the recursion:

$$H_k(x) = x \cdot H_{k-1}(x) - k \cdot H_{k-2}(x) \quad (\text{A-24})$$

The magnitude of $H_k(x)$ for large x is bounded by $1.086 \cdot \sqrt{k!} \exp(x^2/4)$ [9].

To avoid overflow problems in the computation of b_k , equation (A-2) may be rewritten as:

$$b_k = \begin{cases} 0, & k \text{ even} \\ K^2 \frac{2}{\pi} \frac{1}{\sigma_x^{2k}} \left[\sum_{p=1}^{\lfloor N/2 \rfloor} \delta_p e^{-(a_p/\sigma_x)^2/2} H'_{k-1}(a_p/\sigma_x) \right]^2, & k \text{ odd} \end{cases} \quad (\text{A-25})$$

where $H'_k(x)$ is defined as:

$$H'_k \equiv \frac{H_k(x)}{\sqrt{k!}} \quad (\text{A-26})$$

which may be efficiently computed recursively using:

$$\begin{aligned} H'_0(x) &= 1 \\ H'_1(x) &= x \\ H'_k(x) &= \frac{1}{\sqrt{k}} \left[x H'_{k-1}(x) - \sqrt{k-1} H'_{k-2}(x) \right] \end{aligned} \quad (\text{A-27})$$

The quantizer gain coefficient \bar{K} is defined in equation (A-13) and represents a required gain factor for a real quantizer with unit power, zero-mean Gaussian input to provide an output also with unit power. Although as indicated in (A-13), this coefficient may be determined as:

$$\bar{K} = \left(\sum_{k=1}^{\infty} \bar{h}_{0k}^2 / k! \right)^{-1/2} \quad (\text{A-28})$$

numerically, this is somewhat challenging since the series $\{\bar{h}_{0k}\}$ converges slowly with k , especially for quantizers with a small number, N , of output levels.

An alternative approach to determine \bar{K} is to examine the probabilities of occurrence for each of the N quantizer output levels, similar to the analysis to be presented in Appendix B, except with the input to the quantizer approximated as zero-mean.

With unit power, zero-mean Gaussian input a real quantizer with $K = 1$ and an even number of levels has an output variance given by:

$$\begin{aligned} \sigma^2 &= \frac{Q^2}{2} \left(\sum_{p=1}^{N/2-1} (2p-1)^2 \left[\text{erf}(pQ) - \text{erf}((p-1)Q) \right] \right) \\ &\quad + (N-1)^2 \left[\frac{1}{2} - \text{erf} \left(\left(\frac{N}{2} - 1 \right) Q \right) \right] \end{aligned} \quad (\text{A-29})$$

where it is understood that the summation is zero if the upper limit is lower than the lower limit, as is the case for a 1-bit quantizer ($N = 2$).

With the same input process, a real quantizer with an odd number of levels has an output variance:

$$\sigma^2 = -2Q^2 \sum_{p=1}^{N/2-1} (2p-1) \text{erf} \left(\frac{(2p-1)Q}{2} \right) + \left(\frac{N-1}{2} \right)^2 Q^2 \quad (\text{A-30})$$

Both (A-29) and (A-30) were derived by determining the variance for $N = 2, 3, 4, 5, 6$, and 7 levels and observing the patterns that emerged with increasing N .

Finally, the alternate expression for \bar{K} is:

$$\bar{K} = \frac{1}{\sigma} \quad (\text{A-31})$$

using (A-29) or (A-30) as appropriate. This result is also useful to determine the degree of convergence obtained by truncating the series $\{\bar{h}_{0k}\}$ to a finite number of terms, since the following should hold:

$$\sum_{k=1}^{\infty} \bar{h}_{0k}^2 / k! = \sigma^2 \quad (\text{A-32})$$

APPENDIX B: DERIVATION OF MEAN VALUE AND VARIANCE OF CORRELATION SUMS

The mean value of each correlation sum is:

$$E[z_k] = \frac{1}{M} \sum_{n=kM}^{(k+1)M-1} E[\tilde{r}_n^q s_n^*] e^{-j\phi} \quad (\text{B-1})$$

Using the cyclostationary model for the desired signal can be expanded as:

$$\begin{aligned} E[z_k] &= \frac{1}{M} \sum_{n=kM}^{(k+1)M-1} E \left[E[\tilde{r}_n^q | s_n] s_n^* \right] e^{-j\phi} \\ &= \frac{1}{M} \sum_{n=kM}^{(k+1)M-1} E \left[\left(E[\tilde{x}_n^q | s_n] + j E[\tilde{y}_n^q | s_n] \right) s_n^* \right] e^{-j\phi} \end{aligned} \quad (\text{B-2})$$

where the inner expectation is with respect to \tilde{r}_n^q , and the outer expectation is with respect to s_n . (see, e.g., [13, Section 3.2] for a discussion of this expanded form of the expectation operator).

The real and imaginary components of \tilde{r}_n^q each are constrained to only a finite number of levels (the N real quantizer output levels) so that the inner expectations in equation (B-2) involve finite summations, e.g.,

$$E[\tilde{x}_n^q | s_n] = \sum_{p=1}^{\lfloor N/2 \rfloor} o_p \left(P[\tilde{x}_n^q = o_p | s_n] - P[\tilde{x}_n^q = -o_p | s_n] \right) \quad (\text{B-3})$$

where o_p is the p -th positive quantizer output level given by

$$o_p = K \sum_{q=1}^p \delta_p \quad (\text{B-4})$$

and the odd symmetry of the real quantizer has been utilized. Since the input to each real quantizer is Gaussian-distributed, the probabilities in (B-3) are readily computed as, e.g.,:

$$\begin{aligned} P[\tilde{x}_n^q = o_p | s_n] &= P[a_p' < \tilde{x}_n \leq a_{p+1}' | s_n] \\ &= \text{erf} \left(\frac{a_p' - \sqrt{C} \text{Re}[\tilde{s}_n e^{j\phi}]}{\sigma_{\tilde{x}}} \right) \\ &\quad - \text{erf} \left(\frac{a_{p-1}' - \sqrt{C} \text{Re}[\tilde{s}_n e^{j\phi}]}{\sigma_{\tilde{x}}} \right) \end{aligned} \quad (\text{B-5})$$

where

$$\text{erf}(x) \equiv \frac{1}{\sqrt{2\pi}} \int_0^x \exp(-t^2/2) dt \quad (\text{B-6})$$

and $\{a_p'\}$ is an extension of $\{a_p\}$ defined in equations (15) and (16):

$$a_p' = \begin{cases} a_p, & p \leq \lfloor N/2 \rfloor \\ \infty, & p > \lfloor N/2 \rfloor \end{cases} \quad (\text{B-7})$$

By the low input signal-to-noise ratio assumption in equation (9), it follows that $|\sqrt{C}\tilde{s}_n/\sigma_{\tilde{x}}| \ll 1$ and the approximation

$$\text{erf}(x + \Delta x) \approx \text{erf}(x) + \frac{e^{-x^2/2}}{\sqrt{2\pi}} \Delta x \quad (\text{B-8})$$

for $|\Delta x| \ll 1$ may be applied to (B-5) resulting in:

$$\begin{aligned} E[\tilde{x}_n^q | s_n] &= \sum_{p=1}^{\lfloor N/2 \rfloor} o_p (P[a_p' < \tilde{x}_n \leq a_{p+1}' | s_n] - P[-a_{p+1}' < \tilde{x}_n \leq a_p' | s_n]) \\ &= \sqrt{\frac{2}{\pi}} \frac{\sqrt{C} \text{Re}[\tilde{s}_n e^{j\phi}]}{\sigma_{\tilde{x}}} \sum_{p=1}^{\lfloor N/2 \rfloor} o_p \left[e^{-\frac{1}{2}(a_p'/\sigma_{\tilde{x}})^2} - e^{-\frac{1}{2}(a_{p+1}'/\sigma_{\tilde{x}})^2} \right] \\ &= \sqrt{\frac{2}{\pi}} \frac{\sqrt{C} \text{Re}[\tilde{s}_n e^{j\phi}]}{\sigma_{\tilde{x}}} \sum_{p=1}^{\lfloor N/2 \rfloor} o_p e^{-\frac{1}{2}(a_p'/\sigma_{\tilde{x}})^2} - \sum_{p=1}^{\lfloor N/2 \rfloor - 1} o_p e^{-\frac{1}{2}(a_{p+1}'/\sigma_{\tilde{x}})^2} \\ &= \sqrt{\frac{2}{\pi}} \frac{\sqrt{C} \text{Re}[\tilde{s}_n e^{j\phi}]}{\sigma_{\tilde{x}}} \sum_{p=1}^{\lfloor N/2 \rfloor} o_p e^{-\frac{1}{2}(a_p'/\sigma_{\tilde{x}})^2} - \sum_{p=2}^{\lfloor N/2 \rfloor} o_{p-1} e^{-\frac{1}{2}(a_p'/\sigma_{\tilde{x}})^2} \\ &= \sqrt{\frac{2}{\pi}} \frac{\sqrt{C} \text{Re}[\tilde{s}_n e^{j\phi}]}{\sigma_{\tilde{x}}} \sum_{p=2}^{\lfloor N/2 \rfloor} [o_p - o_{p-1}] e^{-\frac{1}{2}(a_p'/\sigma_{\tilde{x}})^2} + o_1 e^{-\frac{1}{2}(a_1/\sigma_{\tilde{x}})^2} \\ &= \sqrt{\frac{2}{\pi}} \frac{\sqrt{C} \text{Re}[\tilde{s}_n e^{j\phi}]}{\sigma_{\tilde{x}}} \sum_{p=1}^{\lfloor N/2 \rfloor} K \delta_p e^{-\frac{1}{2}(a_p/\sigma_{\tilde{x}})^2} \\ &= K \cdot h_{01} \cdot \sqrt{C} \cdot \text{Re}[\tilde{s}_n e^{j\phi}] \end{aligned} \quad (\text{B-9})$$

Using (A-12) and (A-13), (B-9) can also be expressed as:

$$E[\tilde{x}_n^q | s_n] = \bar{K} \cdot \bar{h}_{01} \cdot \sqrt{C} \cdot \text{Re}[\tilde{s}_n e^{j\phi}] \quad (\text{B-10})$$

Similarly, an expression for the mean value of \tilde{y}_n^q may be determined as:

$$E[\tilde{y}_n^q | s_n] = \bar{K} \cdot \bar{h}_{01} \cdot \sqrt{C} \cdot \text{Im}[\tilde{s}_n e^{j\phi}] \quad (\text{B-11})$$

and finally, substituting (B-10) and (B-11) into (B-2):

$$\begin{aligned} E[z_k] &= \frac{1}{M} \sum_{n=kM}^{(k+1)M-1} E \left[E[\tilde{x}_n^q | s_n] s_n^* \right] e^{-j\phi} \\ &= \bar{K} \cdot \bar{h}_{01} \cdot \sqrt{C} \cdot \frac{1}{M} \sum_{n=kM}^{(k+1)M-1} E[\tilde{s}_n s_n^*] \end{aligned} \quad (\text{B-12})$$

which leads directly to equation (26) in the main body of this paper.

The variance of the k -th complex correlator output is:

$$\text{var}[z_k] = E[|z_k|^2] - |E[z_k]|^2 \quad (\text{B-13})$$

The mean value of the k -th complex correlator output, z_k , was determined previously in equation (B-12). However, note that in the derivation of the autocorrelation and power spectral density of the complex quantizer, equations (18) and (23), respectively, the mean value of the input to the quantizer (the desired signal term) was noted to be very small relative to the variance of the input (noise and interference terms) and approximated as zero. To maintain consistency with this earlier approximation, the variance of z_k is thus approximated as:

$$\begin{aligned} \text{var}[z_k] &\approx E \left[|z_k|^2 \right]_{\text{desired signal absent}} \\ &= E \left[\frac{1}{M} \sum_{n=kM}^{(k+1)M-1} \tilde{x}_n^q s_n^* e^{-j\phi} \frac{1}{M} \sum_{m=kM}^{(k+1)M-1} (\tilde{x}_m^q)^* s_m e^{j\phi} \right] \\ &= \frac{1}{M^2} \sum_{n=kM}^{(k+1)M-1} \sum_{m=kM}^{(k+1)M-1} E \left[E[\tilde{x}_n^q (\tilde{x}_m^q)^* | s_n, s_m^*] s_n s_m^* \right] \\ &= \frac{1}{M^2} \sum_{n=kM}^{(k+1)M-1} \sum_{m=kM}^{(k+1)M-1} R_{\tilde{x}^q}[n-m] E[s_n s_m^*] \\ &= \frac{1}{M^2} \sum_{n=kM}^{(k+1)M-1} \sum_{m=kM}^{(k+1)M-1} R_{\tilde{x}^q}[n-m] R_s[m; n-m] \\ &= \frac{1}{M^2} \sum_{n=(M-1)}^{M-1} R_{\tilde{x}^q}[n] \sum_{m=0}^{M-|n|-1} R_s[m+kM; n] \end{aligned} \quad (\text{B-14})$$

For large M , equation (B-14) simplifies to:

$$\text{var}[z_k] = \frac{1}{M} \sum_{n=(M-1)}^{M-1} R_{\tilde{x}^q}[n] R_s[n] \left(1 - \frac{|n|}{M} \right) \quad (\text{B-15})$$

If the coherent correlation interval is large relative to the desired signal spreading symbol rate, i.e., $MT_s \gg T_c$, then (B-15) may be further approximated by:

$$\begin{aligned} \text{var}[z_k] &\approx \frac{1}{M} \sum_{n=(M-1)}^{M-1} R_{\tilde{x}^q}[n] R_s[n] \\ &= \frac{1}{M} \frac{1}{2\pi} \int_{\omega=-\pi}^{\pi} S_{\tilde{x}^q}(e^{j\omega}) S_s(e^{j\omega}) d\omega \end{aligned} \quad (\text{B-16})$$

which involves the inner product between the power spectral density of the complex quantizer output due to noise and interference and the power spectral density of the normalized desired signal. The above derivation closely parallels the development of correlator output variance with analog signal processing, e.g., see [14].

ACKNOWLEDGMENTS

The author would like to thank Dr. Alex Cerruti for graciously providing the simulation results. This work was funded by the Federal Aviation Administration.

REFERENCES

- [1] Spilker, James J., Jr., *Digital Communications by Satellite*, Englewood Cliffs, NJ: Prentice-Hall, 1977.
- [2] Chang, H., "Presampling Filtering, Sampling and Quantization Effects on the Digital Matched Filter Performance," *Proceedings of the International Telemetry Conference*, San Diego, California, 1982, pp. 889 - 915.
- [3] Van Dierendonck, A. J., "GPS Receivers," in B. Parkinson, J. J. Spilker, Jr., Eds., *Global Positioning System: Theory and Applications, Vol. I*, Washington, D.C.: American Institute of Aeronautics and Astronautics, 1996.
- [4] Ward, P., J. Betz, and C. Hegarty, "Interference, Multipath, and Scintillation," in *Understanding GPS: Principles and Applications*, 2nd Ed., Kaplan, E., and C. Hegarty, Eds., Norwood, MA: Artech House, 2006.
- [5] Betz, John W., and Nathan Schnidman, "Receiver Processing Losses with Bandlimiting and One-Bit Quantization," *Proceedings of The Institute of Navigation ION-GNSS-2007*, Fort Worth, Texas, September 2007.
- [6] Betz, John W., "Bandlimiting, Sampling, and Quantization for Modernized Spreading Modulations in White Noise," *Proceedings of The Institute of Navigation National Technical Meeting*, San Diego, January 2008, pp. 980 - 991.
- [7] Thomas, J. B., *Functional Description of Signal Processing in the Rogue GPS Receiver*, National Aeronautics and Space Administration Jet Propulsion Laboratory, JPL Publication 88-15, Pasadena, California, June 1, 1988.
- [8] Akos, Dennis M., and Marco Pini, "Effect of Sampling Frequency on GNSS Receiver Performance," *NAVIGATION: Journal of The Institute of Navigation*, Vol. 53, No. 2, Summer 2006, pp. 85 – 95.
- [9] Hurd, William J., "Correlation Function of Quantized Sine Wave Plus Gaussian Noise," *IEEE Transactions on Information Theory*, Vol. IT-13, No. 1, January 1967, pp. 65 – 68.
- [10] Davenport, Jr., W. B., and W. L. Root, *Random Signals and Noise*, New York: McGraw-Hill, 1958.
- [11] Van Vleck, J. H., and David Middleton, "The Spectrum of Clipped Noise," *Proceedings of the IEEE*, Vol. 54, No. 1, January 1966, pp. 2 – 19.
- [12] Proakis, J., *Digital Communications*, New York: McGraw-Hill, 1995.
- [13] Stark, Henry, and John W. Woods, *Probability, Random Processes, and Estimation Theory for Engineers*, Englewood-Cliffs, New Jersey: Prentice-Hall, 1986.
- [14] Hegarty, C., Y. Lee, and M. Tran, "Simplified Techniques for Analyzing the Effects of Non-white Interference on GPS Receivers," *Proceedings of ION GPS 2002*, Portland, Oregon, 2002.